Selectivity of Malachite Green on Cationic Dye Mixtures Toward Adsorption on Magnetite Humic Acid

Nur Ahmad[1,3], Fitri Suryani Arsyad[2], Idha Royani[2], and Aldes Lesbani[2,3*]

[1]Magister Program in Environment Management, Sriwijaya University, Jl. Padang Salasa No. 524 Ilir Barat 1, Palembang 30139, South Sumatera, Indonesia
[2]Graduate School, Faculty of Mathematics and Natural Sciences, Sriwijaya University, Jl. Palembang-Prabumulih, Km.90-32, Ogan Ilir, South Sumatera, Indonesia
[3]Research Center of Inorganic Center of Inorganic Materials and Complexes, Faculty of Mathematics and Natural Sciences, Sriwijaya University, Jl. Padang Salasa No. 524 Ilir Barat 1, Palembang 30139, South Sumatera, Indonesia

ARTICLE INFO

Received: 29 Jun 2022
Received in revised: 31 Jul 2022
Accepted: 8 Aug 2022
Published online: 7 Sep 2022
DOI: 10.32526/ennrj/20/202200142

Keywords:
Magnetite/ Humic acid/ Selectivity/ Malachite green/ Adsorption

*** Corresponding author:**
E-mail:
aldeslesbani@pps.unsri.ac.id

ABSTRACT

Magnetite humic acid (MHA) was successfully synthesized by the coprecipitation method followed by hydrothermal process, as evidenced by the XRD, FTIR, VSM, and SEM analysis characterization results. XRD diffraction shows diffraction peaks at 2θ=21.53º, 35.95º, and 57.93º. The FTIR spectra have a typical absorption at 3,410, 1,589, 1,396, 1,026, 910, 794, and 540 cm^{-1}. Magnetite humic acid was paramagnetic with magnetization (Ms) 17.04 emu/g. Humic acid and magnetite humic acid have an irregular structure; the morphology of magnetite humic acid is smoother than humic acid. Malachite green was more selective than methylene blue and rhodamine B on magnetite humic acid. The adsorption of malachite green on humic acid and magnetite humic acid was carried out at pH_{pzc} 8.06 and 6.08. The adsorption capacity (Q_{max}) of humic acid (77.519 mg/g) and magnetite humic acid (169.492 mg/g) were found with pseudo-second-order kinetic and Langmuir isotherm models. After five regeneration cycles, the adsorption percentages of malachite green with humic acid and magnetite humic acid ranged from 94.67-61.37% and 62.03-21.11%, respectively. Magnetite humic acid has high stability and reusability. The good regeneration of MHA was supported by the XRD diffractogram. Magnetic properties in the material simplify the adsorption process and minimize the potential for damage to the surface of the material.

1. INTRODUCTION

Textile wastewater is a severe problem for the environment. Textile wastewater pollutes water, which is a basic human need. The industrial sector uses 100,000 dyes to generate textile wastewater (Fazal et al., 2018; Khalaf, 2008). However, only 8% of Textile wastewater is treated before being discharged into waters (Roohi et al., 2016). Wastewater is dangerous for the environment and human health because of the carcinogenic effects caused by these dyes. Malachite green (MG) dye is used in textile and paper industries, and even in food coloring additives (Srivastava et al., 2004). Malachite green can cause disturbances in the immune and reproductive systems (Das and Dhar, 2020) and even cause kidney failure (Eltaweil et al., 2020).

There are different technologies for removing dyes from textile wastewater, such as membrane (Januário et al., 2022), electrocoagulation (Signorelli et al., 2021), photocatalytic (You et al., 2022), and adsorption (Sachdev et al., 2022; Zhang et al., 2020). The adsorption process is suitable for its simplicity, effectivness, efficiency, and low cost. Several adsorbents have been reported, including kaolin (Angerasa et al., 2021), bentonite (Wang et al., 2021a), layer double hydroxide (Lesbani et al., 2020; Wijaya et al., 2021), and humic acid (Yang and Antonietti, 2020).

Humic acid (HA) is extracted from peat soil with -COOH and -OH groups (Stevenson, 1994). Humic acid is one of the fractions of humic compounds that are naturally occurring in soil organic matter. Humic acid (HA) has the potential for

Citation: Ahmad N, Arsyad FS, Royani I, Lesbani A. Selectivity of malachite green on cationic dye mixtures toward adsorption on magnetite humic acid. Environ. Nat. Resour. J. 2022;20(6):634-643. (https://doi.org/10.32526/ennrj/20/202200142)

adsorption because of its high adsorption capacity, and use in organic and inorganic pollutants (Shao et al., 2021). However, the structure of humic acid is easily damaged and difficult to separate from aqueous solution. Magnetite (Fe_3O_4) is an iron oxide of the spinel mineral group (She et al., 2021). Magnetite has been applied to adsorption for water treatment (Abdullah et al., 2022; Paz et al., 2022), catalysts (Liu et al., 2018), membrane processes (Vu et al., 2020), and biodegradation (Shen et al., 2021). Magnetite, in adsorption, imparts its magnetic properties to HA, and it can separate the adsorbent from the solution using an external magnet (Lee and Kim, 2022). Composite magnetite with humic acid (MHA) has been reported for removing phosphate (Rashid et al., 2017), gold ion adsorption (Santosa et al., 2021a), and removing Pb(II) (Lu et al., 2019). Selectivity and adsorption of MHA for malachite green has not been registered.

In this study, Magnetite Humic Acid (MHA) was synthesized by the conventional coprecipitation method followed by hydrothermal process as evidenced by the characterization results using XRD, FTIR, VSM, and SEM analysis. A selectivity test was performed by mixing cationic dyes to determine the dye used for the adsorption process. Adsorption processes such as kinetic, isotherm, and thermodynamic, and the stability of the adsorbent with regeneration were evaluated.

2. METHODOLOGY

2.1 Materials and instruments

Humic acid (HA) was extracted from the peat soil of South Sumatra, Indonesia. Chemicals (analytical-grade reagent) used in this study, $FeCl_3$ (Merck, 162.2 g/mol), $FeSO_4{\cdot}7H_2O$ (Merck, 278.01 g/mol), HCl (MallinckrodtAR®, 37%), NaOH (40 g/mol), and NH_3 (25%) were purchased from EMSURE® ACS. Distilled water was purchased from PT. Bratachem Indonesia. Analytical instrumentals used included UV-Vis Spectrophotometer type Biobase BK-UV 1800 PC (China), Fourier Transfer Infra-Red (FTIR, Japan) type Shimadzu Prestige-21, X-Ray Diffractometer (XRD, Japan) type Rigaku Miniflex-6000, Vibrating Sample Magnetometer (VSM, England) type OXFORD VSM1.2H, and FEI Quanta 650 Scanning Electron Microscope (SEM, England) OXFORD.

2.2 Synthesis of magnetite humic acid (MHA)

MHA was synthesized by coprecipitation method followed by hydrothermal process (Taher et al., 2021). $FeCl_3$ (0.6488 g) and $FeSO_4{\cdot}7H_2O$ (0.5560 g) was added to 6 mL of distilled water, then stirred until dissolved. The mixture was added to 1 g of humic acid (HA) and stirred for 3 h at room temperature. NH_3 (3 mL) was added to the mixture slowly, then stirred for 30 min at 75ºC. The obtained slurry was transferred to Teflon for hydrothermal treatment for 3 h at 150ºC. The slurry was washed and then dried at 100ºC.

2.3 Determination of functional group of HA and MHA

2.3.1 Total acidity

HA (0.1 g) or MHA (0.1 g) were added to $Ba(OH)_2$ saturated solution (20 mL) under N_2 atmosphere and stirred for 24 h at 25ºC. Afterward, the HA or MHA treated was filtered using Whatman paper and washed with distilled water. The filtrate and wash water were combined and then titrated with HCl (0.5 M) to pH 8.4 (Santosa et al., 2021a). The total acidity of HA and MHA was then calculated by Equation (1):

$$\text{Total acidity (cmol/kg)} = \frac{(V_0 - V_s) \times M \times 10^5}{W} \quad (1)$$

Where; V_0 and V_s are the volume of HCl for titrated blank solution and sample, respectively; M is the molarity of HCl; W is the mass of HA and MHA.

2.3.2 Carboxyl content

HA (0.1 g) or MHA (0.1 g) were added to the mixture of $Mg(CH_3COO)_2$ 0.5 M (10 mL) and distilled water (40 mL) under N_2 atmosphere and stirred for 24 h at 25ºC. Afterward, the treated HA or MHA was filtered using Whatman paper and washed with distilled water. The filtrate and wash water were combined then titrated with NaOH (0.1 M) to pH 9.8 (Santosa et al., 2021a). The carboxyl content was determined using Equation (2):

$$\text{Carboxyl content (cmol/kg)} = \frac{(V_0 - V_s) \times M \times 10^5}{W} \quad (2)$$

Where; V_0 and V_s are the volume of NaOH for titrated blank solution and sample, respectively; M is the molarity of NaOH; W is the mass of HA and MHA.

2.3.3 Phenolic hydroxyl content

Phenolic hydroxyl content is the difference between total acidity and carboxyl content. Phenolic hydroxyl content was determined using Equation (3):

$$\text{Phenolic hydroxyl content (cmol/kg)} = \text{Total acidity} - \text{Carboxyl content} \quad (3)$$

2.4 Selectivity of cationic dye mixture

Selectivity was carried out to determine the most adsorbed dye by the adsorbent. Selectivity was performed using a mixture of 25 mg/L of rhodamine B, malachite green, and methylene blue. HA and MHA (20 mg) were added to 20 mL of the cationic dye mixture and shaken for 15, 30, 60, 90, 120, and 150 min. The absorbance was measured at the wavelength scan.

2.5 Determination of pH_{pzc} of MHA

pH_{pzc} of HA and MHA was determined by the conventional pH-drift method. HA and MHA (20 mg) were added to 20 mL of 1 M NaCl at various pH from 2 to 11 (Tombácz and Szekeres, 2004). HCl 0.1 M or NaOH 0.1 M was added to adjust the initial pH of the NaCl. Then, the mixture was shaken for 24 h. The final pH of each NaCl was measured.

2.6 Adsorption of malachite green

2.6.1 Adsorption kinetics

HA and MHA (20 mg) were added into 20 mL of malachite green with 60 mg/L, which had been adjusted at pH_{pzc}. Stirring is done with time variations of 10, 20, 30, 40, 50, 60, 70, 90, 120, 150, and 180 min in each beaker at 303 K. After stirring at 100 rpm, MHA was separated from the malachite green using an external magnet. The dye solution has been separated is then measured its absorbance using a UV-Vis at 617 nm. The adsorption kinetics were analyzed by pseudo-first-order (PFO) and pseudo-second-order (PSO) with the following Equations 4 and 5, respectively.

$$\log(Q_e - Q_t) = \log Q_e - \left(\frac{k_1}{2.303}\right) t \quad (4)$$

$$\frac{1}{Q_t} = \frac{1}{k_2 Q_e^{\,2}} + \frac{1}{Q_e} \quad (5)$$

Where; Q_e and Q_t are adsorption capacity at equilibrium and t, respectively (mg/g); k_1 (min^{-1}) and k_2 (g/mg/min) are the rate constant at PFO and PSO, respectively; t is the adsorption time of malachite green (min).

2.6.2 Adsorption isotherms

HA and MHA (20 mg) were added into 20 mL of malachite green with 50, 75, 100, 150, 175, and 200 mg/L, which had been adjusted at pH_{pzc} - stirring for 2 h with various temperatures (303, 313, 323, 333, and 343 K) in each beaker. After stirring at 100 rpm, MHA was separated from the malachite green using an external magnet. The adsorption isotherms were analyzed by Langmuir and Freundlich isotherms model with the following Equations 6 and 7, respectively.

$$\frac{C_e}{Q_e} = \frac{C_e}{Q_m} + \frac{1}{Q_m K_L} \quad (6)$$

$$\log Q_e = \log K_F - {}^{1}/_{n} \log C_e \quad (7)$$

Where; C_e (mg/L) and Q_e (mg/g) are the concentration of malachite green and adsorption capacity at equilibrium, respectively (mg/g); Q_m (mg/g) is the maximum adsorption capacity; K_L and K_F are the rate constant at Langmuir and Freundlich, respectively.

The thermodynamic equation and the Gibbs free energy were determined using Equations 8 and 9, respectively.

$$\ln \frac{Q_e}{C_e} = \frac{\Delta S}{R} - \frac{\Delta H}{RT} \quad (8)$$

$$\Delta G° = \Delta H - T\Delta S \quad (9)$$

Where; C_e (mg/L) and Q_e (mg/g) are the concentration of malachite green and adsorption capacity at equilibrium, respectively (mg/g); ΔS (J/mol.K) is the entropy; $\Delta G°$ (kJ/mol) is the Gibbs free energy. ΔH (kJ/mol) is the enthalpy; R (J/mol/K) is the gas constant; T (K) is the temperature.

2.6.3 Regeneration of MHA

HA and MHA (20 mg) were added to 20 mL of malachite green with a concentration of 80 mg/L adjusted at pH_{pzc}. Stirring was carried out for 2 h at 303 K. After the stirring process is complete, the adsorbent is separated from the adsorbate. After that, the desorption process (distilled water medium) was carried out to remove the dye from the adsorbent. HA and MHA were reused two to five times in the adsorption and desorption processes.

3. RESULTS AND DISCUSSION

3.1 Characteristics of HA and MHA

XRD diffractogram of HA as shown in Figure 1(a) 21.53º, 25.03º, 35.75º, 55.08º, and 62.31º. XRD diffraction of MHA shows diffraction peaks at 2θ=21.53º, 35.95º, and 57.93º. The diffraction peaks that appear at 2θ=21.53º (002) indicate the presence of high amounts of carbon contained in humic acid

(Zhang et al., 2018). The diffraction peaks at 2θ=35.75º (311) and 57.93º (511) are originally peaks from Magnetite (Santosa et al., 2021b).

The FT-IR spectra of HA and MHA are shown in Figure 1(b). HA has a typical absorption at 3,410 cm^{-1} related to OH group stretching from phenolic hydroxyl content (Ahmad et al., 2022), 1,589 cm^{-1} as C=C stretching, 1,396 and 1,026 cm^{-1} indicated as C-O stretching in COO- (carboxyl content) (Anjum et al., 2019). The peak at 910 cm^{-1} is related to C=C bending and 540 cm^{-1} indicating the presence of metal ions in HA. After HA was modified with magnetite (MHA) at 540 cm^{-1}, the absorption became sharper indicating the presence of Fe-O. A new peak was observed at wavenumber 794 cm^{-1} due to the interaction between C-O and Fe-O.

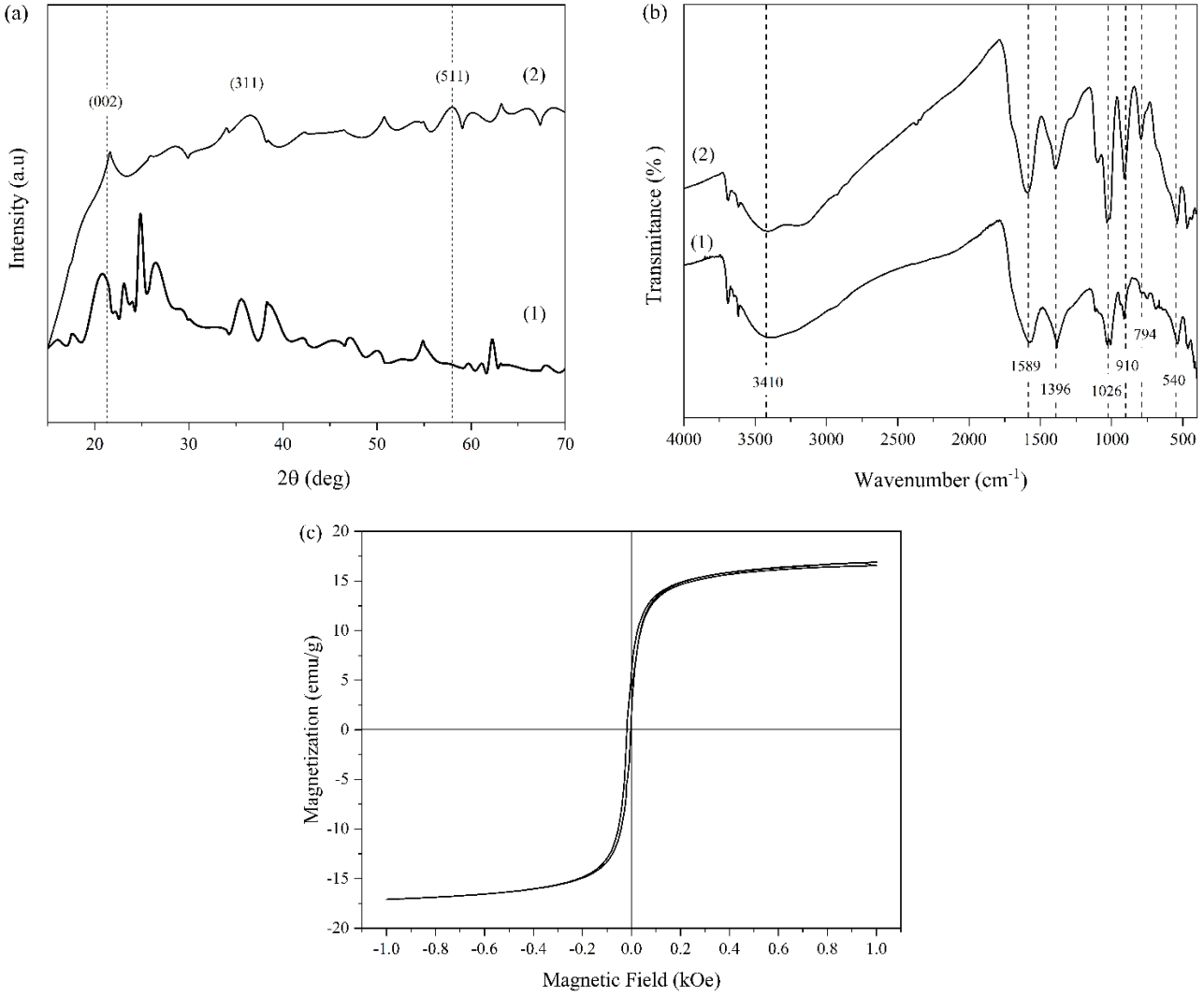

Figure 1. XRD diffractogram (a) and IR spectra (b) of (1) HA, (2) MHA. The measured room temperature magnetization curve of MHA (c)

The magnetic curve of MHA was measured using VSM. Figure 1(c) showed MHA was paramagnetic with magnetization (Ms) 17.04 emu/g. The magnetization (Ms) MHA was lower than Fe_3O_4 (66.3 emu/g) because Fe_3O_4 was classified as superparamagnetic (Santosa et al., 2021b). Figure 2 shows the surface morphology of HA and MHA by SEM images. HA and MHA have irregular structures. The morphology of MHA is smoother than HA. The surface of MHA is smooth because it is synthesized by hydrothermal process.

3.2 Determination of functional group of HA and MHA

Total acidity and carboxylic content were determined by titration using $Ba(OH)_2$ saturated solution and $Mg(CH_3COO)_2$, respectively (Stevenson, 1994). The total acidity, carboxyl content, and Phenolic -OH of HA and MHA are displayed in Table

1. MHA had a drastic decrease in the total acidity and carboxyl content, respectively, from 670 cmol/kg to 317.50 cmol/kg and 296 cmol/kg to 59.33 cmol/kg. This is due to the preparation of MHA carried out under alkaline conditions (addition of NH_3). The carboxyl content and phenolic -OH are iodized and then interact with positively charged Fe^{2+} and Fe^{3+} form Fe_3O_4 (Koesnarpadi et al., 2015). However, the carboxyl group more readily interacts with Fe_3O_4 than the phenolic -OH, so the carboxyl group's reduction is very drastic.

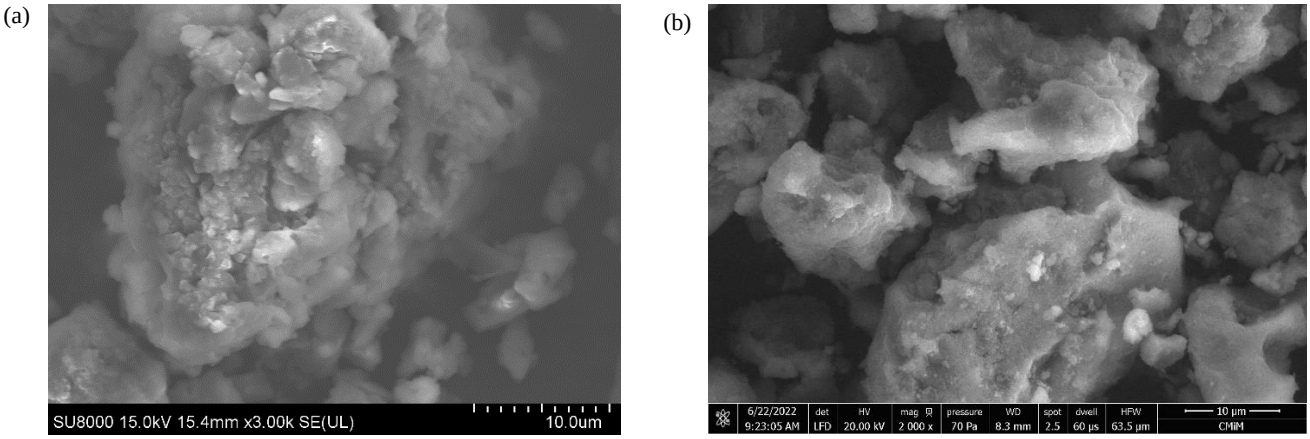

Figure 2. SEM images of HA (a) and MHA (b)

Table 1. Total acidity, carboxyl content, and phenolic -OH of HA and MHA

Functional group	Stevenson (1994) (cmol/kg)	Santosa et al. (2021a) (cmol/kg)		This study (cmol/kg)	
		HA	MHA	HA	MHA
Total acidity	570-890	710.66	320.44	670	317.50
Carboxyl content	150-570	315.79	87.43	296	59.33
Phenolic -OH	150-400	394.87	233.01	374	258.17

3.3 Selectivity adsorbent

Figure 3 shows a wavelength scan for selectivity of malachite green. MHA adsorbed malachite green higher than rhodamine B and methylene blue. The drastic decrease in malachite green concentration indicated that the malachite green structure was smaller than methylene blue and rhodamine B (Mohadi et al., 2021; Palapa et al., 2021). Therefore, malachite green is used for the adsorption process.

3.4 pH_{pzc} of HA and MHA

pH_{pzc} of HA and MHA is the point neither positively nor negatively charged (Derakhshani and Naghizadeh, 2018). Through the movement of H^+ ions from the HA and MHA surface, the pH_{pzc} can be easily measured. Figure 4 shows the movement of H^+ after 24 h in the shaker. At low pH, H^+ moves from the solution to the HA and MHA surface during shaking and increases pH of the solution. At high pH, H^+ moves from the HA and MHA surface to the solution and lowers pH of the solution.

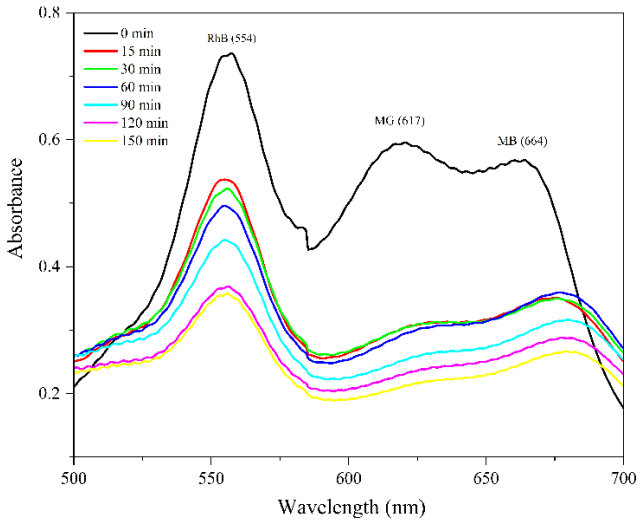

Figure 3. Wavelength scan of adsorption by MHA into a mixture of MG, MB, and RhB

The meeting point between the initial and final pH shows no movement of H^+ ions, which means that this meeting point is that pH_{pzc}. As shown in Figure 4, pH_{pzc} of HA and MHA were at pH 8.08 and 6.08, respectively. In a solution with a pH less than pH_{pzc}, HA, and MHA are positively charged and at pH higher than pH_{pzc}, HA, and MHA are negatively charged.

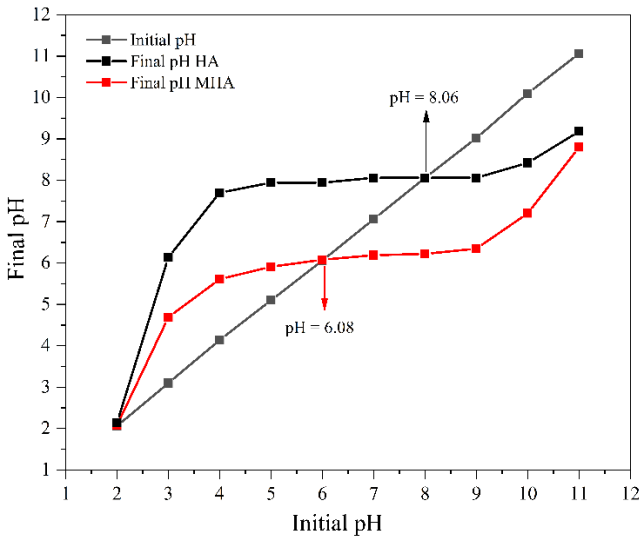

Figure 4. pH_{pzc} of HA and MHA

3.5 Adsorption of malachite green

Figure 5(a) shows that the adsorbed concentration of malachite green increased with time and was constant at 120 min. Pseudo-first-order and pseudo-second-order kinetic adsorption parameters of malachite green are shown in Table 2. The data in Table 2 shows that the value of the coefficient correlation in the adsorption process of malachite green using HA and MHA adsorbent tends to be a pseudo-second-order. The coefficient correlation (R^2) for pseudo-second-order is higher than pseudo-first-order. It means that the greater the concentration of the malachite green, the more adsorbed. Therefore, the adsorption process can be followed by chemisorption (Liu et al., 2020; Siraorarnroj et al., 2022).

Based on Table 2 and Figures 5(b) and 5(c), the coefficient correlation (R^2) of HA and MHA for Langmuir isotherm is higher than Freundlich isotherm at temperature 303 K. The adsorption process tends to follow the Langmuir isotherm. Therefore, the adsorption process can be followed by monolayer adsorption (Wang et al., 2021b). Adsorption capacity (Q_{max}) of HA and MHA was 77.519 and 169.492 mg/g, respectively. Adsorption of malachite green by several adsorbents is shown in Table 3.

Table 2. Kinetic and isotherm model parameter of adsorption on MHA

Kinetic parameter	Parameter	Adsorbent	
		HA	MHA
Pseudo-first-order	Qe_{exp} (mg/g)	41.981	56.075
	Qe_{calc} (mg/g)	52.918	78.289
	k_1 (min^{-1})	0.002	0.002
	R^2	0.980	0.966
Pseudo-second-order	Qe_{exp} (mg/g)	41.981	56.075
	Qe_{calc} (mg/g)	54.945	71.942
	k_2 (g/mg/min)	0.0004	0.0003
	R^2	0.990	0.990
Isotherm parameter	Parameter	Adsorbent	
		HA	MHA
Langmuir	Qmax	77.519	169.492
	kL	0.047	0.042
	R^2	0.968	0.992
Freundlich	N	1.294	2.396
	kF	3.105	21.617
	R^2	0.866	0.935

Table 3. Comparison of HA and MHA with several adsorbents in terms of the adsorption capacity of malachite green

Adsorbent	Q_{max} (mg/g)	Reference
Date stones	98	Hijab et al. (2021)
CuCr-[α-$SiW_{12}O_{40}$]	55.322	Palapa et al. (2020)
ZIF-8@Fe/Ni	151.520	Zhang et al. (2021)

Table 3. Comparison of HA and MHA with several adsorbents in terms of the adsorption capacity of malachite green (cont.)

Adsorbent	Q_{max} (mg/g)	Reference
Chitosan-DES B	17.86	Sadiq et al. (2020)
EPS of *Lysinibacillus* sp. SS1	178.57	Miyar et al. (2021)
GALA	113.5	Chen et al. (2020)
Plasma-based biomass	15.55	Al-Yousef et al. (2021)
S@TP Biochar	30.18	Vigneshwaran et al. (2021)
Chinese fan palm seed biochar	21.4	Giri et al. (2022)
HA	77.519	This study
MHA	169.492	This study

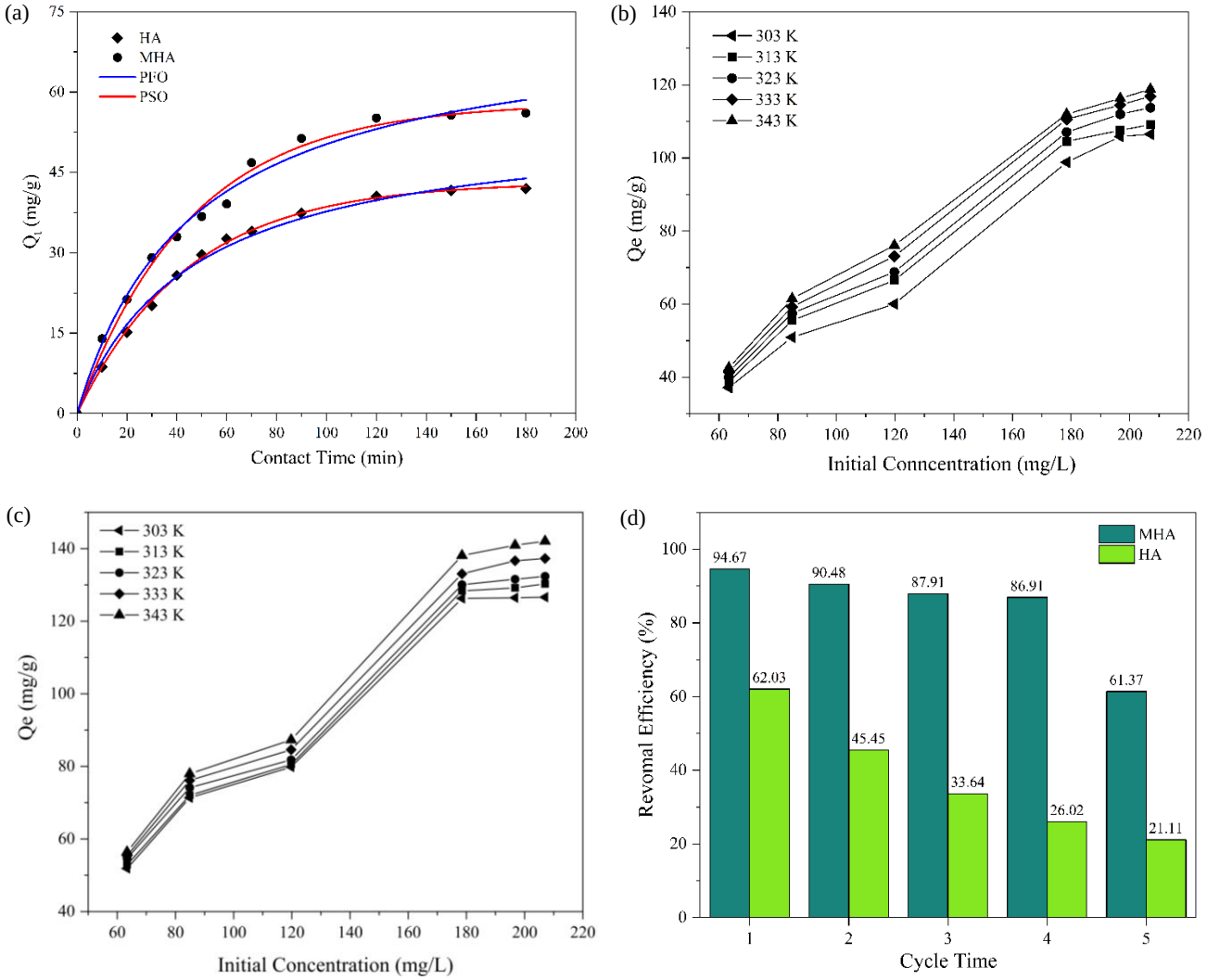

Figure 5. Effect of contact time (a), effect of initial concentration and temperature (b) and (c), regeneration (d) of HA and MHA

Table 4 shows the thermodynamic data of HA and MHA for adsorption of malachite green. The value of ΔG° is negative, meaning that the adsorption takes place spontaneously. ΔH is positive, meaning that the adsorption is endothermic and requires energy for the adsorption process. ΔS is positive, meaning that there is an increase in irregularity on the surface of the adsorbent. Based on Figure 5(d), during five regeneration cycles of HA and MHA, the adsorption percentages of malachite green decreased from 94.6-61.37% and 62.03-21.11%, respectively. Magnetic properties in the material simplify the adsorption process and minimize the potential for damage to the material's surface. MHA has high stability and reusability of adsorbent up to five times. The good regeneration of MHA indicates that MHA has good

Table 4. Adsorption thermodynamic parameter

Adsorbent	ΔH (kJ/mol)	ΔS (kJ/mol)	ΔG (kJ/mol)					R^2
			303 K	313 K	323 K	333 K	343 K	
HA	8.189	0.029	-0.582	-0.871	-1.161	-1.450	-1.740	0.998
MHA	12.940	0.055	-3.764	-4.316	-4.867	-5.418	-5.969	0.988

stability, supported by the XRD diffractogram after adsorption with no significant changes as shown in Figure 6. The diffraction peaks at 2θ=21.53º (002), 35.95º (311), and 57.93º (511) can still be observed. The adsorption mechanism can be studied from electrostatically interacting MHA with the cationic malachite green. In addition, the hydrogen bonding interactions and π-π interactions between the aromatic ring of the malachite green and the MHA can affect the adsorption mechanism.

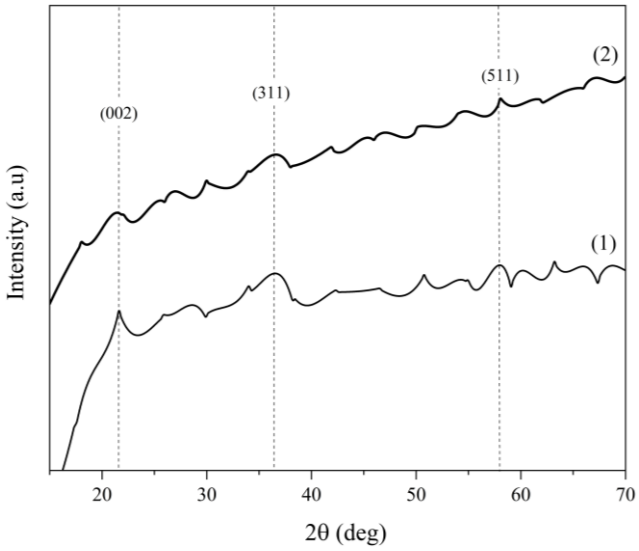

Figure 6. XRD diffractogram of MHA before (1) and after (2) adsorption

4. CONCLUSION

In this study, magnetite humic acid (MHA) was successfully synthesized by the coprecipitation method followed by hydrothermal process. Selectivity of cationic dyes shows that malachite green was more selective than methylene blue and rhodamine B. Malachite green has a smaller structure than methylene blue and rhodamine B. Adsorption capacity (Q_{max}) of HA and MHA was 77.519 and 169.492 mg/g, respectively. After five regeneration cycles, the adsorption percentages of malachite green from HA and MHA ranged from 94.67-61.37% and 62.03-21.11%, respectively. MHA has high stability and reusability as an adsorbent up to five times.

ACKNOWLEDGEMENTS

Authors thank Research Center of Inorganic Materials and Complexes, Faculty of Mathematics and Natural Sciences, Sriwijaya University for instrumental analysis.

REFERENCES

Abdullah TA, Juzsakova T, Mansoor H, Salman AD, Rasheed RT, Hafad SA, et al. Polyethylene over magnetite-multiwalled carbon nanotubes for kerosene removal from water. Chemosphere 2022;287:Article No. 132310.

Ahmad N, Wijaya A, Amri, Fitri ES, Arsyad FS, Mohadi R, et al. Catalytic oxidative desulfurization of dibenzothiophene by composites based Ni/Al-Oxide. Science and Technology Indonesia 2022;7(3):385-91.

Al-Yousef HA, Alotaibi BM, Alanazi MM, Aouaini F, Sellaoui L, Bonilla-Petriciolet A. Theoretical assessment of the adsorption mechanism of ibuprofen, ampicillin, orange G and malachite green on a biomass functionalized with plasma. Journal of Environmental Chemical Engineering 2021;9(1):Article No. 104950.

Angerasa FT, Kalifa MA, Jembere AL, Genet MB. Spent kaolin filter cake as an effective adsorbent for the removal of hexavalent chromium [Cr(VI)] from aqueous solution: Comparative study of wastewater treatment methods. South African Journal of Chemical Engineering 2021;38:90-103.

Anjum H, Johari K, Gnanasundaram N, Appusamy A, Thanabalan M. Investigation of green functionalization of multiwall carbon nanotubes and its application in adsorption of benzene, toluene, and p-xylene from aqueous solution. Journal of Cleaner Production 2019;221:323-38.

Chen H, Liu T, Meng Y, Cheng Y, Lu J, Wang H. Novel graphene oxide/aminated lignin aerogels for enhanced adsorption of malachite green in wastewater. Colloids and Surfaces A: Physicochemical and Engineering Aspects 2020;603:Article No. 125281.

Das KC, Dhar SS. Rapid catalytic degradation of malachite green by $MgFe_2O_4$ nanoparticles in presence of H_2O_2. Journal of Alloys and Compounds 2020;828:Article No. 154462.

Derakhshani E, Naghizadeh A. Optimization of humic acid removal by adsorption onto bentonite and montmorillonite nanoparticles. Journal of Molecular Liquids 2018;259:76-81.

Eltaweil AS, Mohamed HA, El-Monaem EMA, El-Subruiti GM. Mesoporous magnetic biochar composite for enhanced adsorption of malachite green dye: Characterization, adsorption kinetics, thermodynamics and isotherms. Advanced Powder Technology 2020;31(3):1253-63.

Fazal T, Mushtaq A, Rehman F, Khan AU, Rashid N, Farooq W, et al. Bioremediation of textile wastewater and successive biodiesel production using microalgae. Renewable and Sustainable Energy Reviews 2018;82:3107-26.

Giri BS, Sonwani RK, Varjani S, Chaurasia D, Varadavenkatesan T, Chaturvedi P, et al. Highly efficient bio-adsorption of malachite green using Chinese Fan-Palm Biochar (*Livistona chinensis*). Chemosphere 2022;287:Article No. 132282.

Hijab M, Parthasarathy P, Mackey HR, Al-Ansari T, McKay G. Minimizing adsorbent requirements using multi-stage batch adsorption for malachite green removal using microwave date-stone activated carbons. Chemical Engineering and Processing - Process Intensification 2021;167:Article No. 108318.

Januário EFD, Vidovix TB, Calsavara MA, Bergamasco R, Vieira AMS. Membrane surface functionalization by the deposition of polyvinyl alcohol and graphene oxide for dyes removal and treatment of a simulated wastewater. Chemical Engineering and Processing - Process Intensification 2022;170:Article No. 108725.

Khalaf MA. Biosorption of reactive dye from textile wastewater by non-viable biomass of *Aspergillus niger* and *Spirogyra* sp. Bioresource Technology 2008;99(14):6631-4.

Koesnarpadi S, Santosa SJ, Siswanta D, Rusdiarso B. Synthesis and characterizatation of magnetite nanoparticle coated humic acid (Fe_3O_4/HA). Procedia Environmental Sciences 2015; 30:103-8.

Lee WH, Kim JO. Phosphate recovery from anaerobic digestion effluent using synthetic magnetite particles. Journal of Environmental Chemical Engineering 2022;10(1):Article No. 107103.

Lesbani A, Asri F, Palapa NR, Taher T, Rachmat A. Efficient removal of methylene blue by adsorption using composite based Ca/Al layered double hydroxide-biochar. Global Nest Journal 2020;22(2):250-7.

Liu Y, Jia J, Gao T, Wang X, Yu J, Wu D, et al. Rapid, selective adsorption of methylene blue from aqueous solution by durable nanofibrous membranes. Journal of Chemical and Engineering Data 2020;65(8):3998-4008.

Liu Y, Liu Q, Li J, Ngo HH, Guo W, Hu J, et al. Effect of magnetic powder on membrane fouling mitigation and microbial community/composition in membrane bioreactors (MBRs) for municipal wastewater treatment. Bioresource Technology 2018;249:377-85.

Lu M, Zhang Y, Zhou Y, Su Z, Liu B, Li G, et al. Adsorption-desorption characteristics and mechanisms of Pb(II) on natural vanadium, titanium-bearing magnetite-humic acid magnetic adsorbent. Powder Technology 2019;344:947-58.

Miyar HK, Pai A, Goveas LC. Adsorption of malachite green by extracellular polymeric substance of *Lysinibacillus* sp. SS1: Kinetics and isotherms. Heliyon 2021;7(6):e07169.

Mohadi R, Palapa NR, Lesbani A. Preparation of Ca/Al-layered double hydroxides/biochar composite with high adsorption capacity and selectivity toward cationic dyes in aqueous. Bulletin of Chemical Reaction Engineering and Catalysis 2021;16(2):244-52.

Palapa NR, Mohadi R, Rachmat A, Lesbani A. Adsorption study of malachite green removal from aqueous solution using Cu/M^{3+} (M^{3+}=Al, Cr) layered double hydroxide. Mediterranean Journal of Chemistry 2020;10(1):33-45.

Palapa NR, Taher T, Wijaya A, Lesbani A. Modification of Cu/Cr layered double hydroxide by keggin type polyoxometalate as adsorbent of malachite green from aqueous solution. Science and Technology Indonesia 2021;6(3):209-17.

Paz MJ, Vieira T, Enzweiler H, Paulino AT. Chitosan/wood sawdust/magnetite composite membranes for the photo-degradation of agrochemicals in water. Journal of Environmental Chemical Engineering 2022;10(1):Article No. 106967.

Rashid M, Price NT, Pinilla MÁG, O'Shea KE. Effective removal of phosphate from aqueous solution using humic acid coated magnetite nanoparticles. Water Research 2017;123(3):353-60.

Roohi M, Riaz M, Arif MS, Shahzad SM, Yasmeen T, Riaz MA, et al. Varied effects of untreated textile wastewater onto soil carbon mineralization and associated biochemical properties of a dryland agricultural soil. Journal of Environmental Management 2016;183:530-40.

Sachdev D, Shrivastava H, Kajal, Sharma S, Sanjeev, Srivastava S, et al. Potential for hydrothermally separated groundnut shell fibers for removal of methylene blue dye. Materials Today: Proceedings 2022;48:1559-68.

Sadiq AC, Rahim NY, Suah FBM. Adsorption and desorption of malachite green by using chitosan-deep eutectic solvents beads. International Journal of Biological Macromolecules 2020;164:3965-73.

Santosa SJ, Krisbiantoro PA, Ha TTM, Phuong NTT, Gusrizal G. Composite of magnetite and Zn/Al layered double hydroxide as a magnetically separable adsorbent for effective removal of humic acid. Colloids and Surfaces A: Physicochemical and Engineering Aspects 2021b;614:Article No. 126159.

Santosa SJ, Krisbiantoro PA, Yuniarti M, Kustomo, Koesnarpardi S. Magnetically separable humic acid-functionalized magnetite for reductive adsorption of tetrachloroaurate(III) ion in aqueous solution. Environmental Nanotechnology, Monitoring and Management 2021a;15:Article No. 100454.

Shao Y, Bao M, Huo W, Ye R, Liu Y, Lu W. Production of artificial humic acid from biomass residues by a non-catalytic hydrothermal process. Journal of Cleaner Production 2021;335:Article No. 130302.

She HD, Fan HR, Yang KF, Li XC, Wang QW, Zhang LF, et al. In situ trace elements of magnetite in the Bayan Obo REE-Nb-Fe deposit: Implications for the genesis of mesoproterozoic iron mineralization. Ore Geology Reviews 2021;139:Article No. 104574.

Shen X, Dong W, Wan Y, Feng K, Liu Y, Wei Y. Influencing mechanisms of siderite and magnetite, on naphthalene biodegradation: Insights from degradability and mineral surface structure. Journal of Environmental Management 2021;299:Article No. 113648.

Signorelli SCM, Costa JM, Neto AFA. Electrocoagulation-flotation for orange II dye removal: Kinetics, costs, and process variables effects. Journal of Environmental Chemical Engineering 2021;9(5):Article No. 106157.

Siraorarnroj S, Kaewtrakulchai N, Fuji M, Eiad-ua A. High performance nanoporous carbon from mulberry leaves (*Morus alba* L.) residues via microwave treatment assisted hydrothermal-carbonization for methyl orange adsorption: Kinetic, equilibrium and thermodynamic studies. Materialia 2022;21:Article No. 101288.

Srivastava S, Sinha R, Roy D. Toxicological effects of malachite green. Aquatic Toxicology 2004;66(3):319-29.

Stevenson FJ. Humus Chemistry: Genesis, Composition, Reactions. USA: John Wiley and Sons; 1994.

Taher T, Putra R, Palapa NR, Lesbani A. Preparation of magnetite-nanoparticle-decorated NiFe layered double hydroxide and its adsorption performance for congo red dye removal. Chemical Physics Letters 2021;777:Article No. 138712.

Tombácz E, Szekeres M. Colloidal behavior of aqueous montmorillonite suspensions: The specific role of pH in the

presence of indifferent electrolytes. Applied Clay Science 2004;27(1-2):75-94.

Vigneshwaran S, Sirajudheen P, Karthikeyan P, Meenakshi S. Fabrication of sulfur-doped biochar derived from tapioca peel waste with superior adsorption performance for the removal of malachite green and rhodamine B dyes. Surfaces and Interfaces 2021;23:Article No. 100920.

Vu MT, Noori MT, Min B. Conductive magnetite nanoparticles trigger syntrophic methane production in single chamber microbial electrochemical systems. Bioresource Technology 2020;296:Article No. 122265.

Wang M, Li Y, Cui M, Li M, Xu W, Li L, et al. Barium alginate as a skeleton coating graphene oxide and bentonite-derived composites: Excellent adsorbent based on predictive design for the enhanced adsorption of methylene blue. Journal of Colloid and Interface Science 2021a;611:629-43.

Wang Y, Bao S, Liu Y, Yu Y, Yang W, Xu S, et al. CoS_2/GO nanocomposites for highly efficient and ppb level adsorption of Hg(II) from wastewater. Journal of Molecular Liquids 2021b;322:Article No. 114899.

Wijaya A, Siregar PMSBN, Priambodo A, Palapa NR, Taher T, Lesbani A. Innovative modified of Cu-Al/C (C=biochar, graphite) composites for removal of procion red from aqueous solution. Science and Technology Indonesia 2021;6(4):228-34.

Yang F, Antonietti M. Artificial humic acids: Sustainable materials against climate change. Advanced Science 2020;7(5):1-7.

You J, Liu C, Feng X, Lu B, Xia L, Zhuang X. In situ synthesis of ZnS nanoparticles onto cellulose/chitosan sponge for adsorption-photocatalytic removal of congo red. Carbohydrate Polymers 2022;288:Article No. 119332.

Zhang A, Chen W, Gu Z, Li Q, Shi G. Mechanism of adsorption of humic acid by modified aged refuse. RSC Advantages 2018;8:33642-51.

Zhang T, Jin X, Owens G, Chen Z. Remediation of malachite green in wastewater by ZIF-8@Fe/Ni nanoparticles based on adsorption and reduction. Journal of Colloid and Interface Science 2021;594:398-408.

Zhang W, Zhang RZ, Yin Y, Yang JM. Superior selective adsorption of anionic organic dyes by MIL-101 analogs: Regulation of adsorption driving forces by free amino groups in pore channels. Journal of Molecular Liquids 2020; 302:Article No. 112616.